Machine Learning- and SHAP Assisted Experimental Investigation of *Annona reticulata* Bark Fibre–*Prosopis juliflora* Wood–Jamun Seed Powder Hybrid Epoxy Biocomposites

Fairuz Sadaf Shrabon

Department of Mechanical Engineering, The Grove School of Engineering, City College of New York, Manhattan, 275 Convent Ave, New York, USA

Email ID: ammu.phy@gmail.com

Abstract

An integrated experimental and computational framework was developed to investigate epoxy hybrid biocomposites reinforced with *Annona reticulata* bark fibre, *Prosopis juliflora* wood powder and Jamun seed powder. Six formulations, APJ1–APJ6 were fabricated by hand lay-up and evaluated for flexural, tensile, Shore-D hardness, impact and moisture-absorption behaviour. Thermal stability, viscoelastic response, functional groups, crystalline characteristics and fracture morphology were examined using TGA, DMA, FTIR, XRD and SEM, respectively. Among the investigated formulations, APJ5 exhibited the highest tensile and flexural strengths of 267.4 and 341.2 MPa, respectively, whereas APJ6 achieved the highest Shore-D hardness of 85.2, demonstrating property-dependent optimum composition. Machine-learning prediction was performed using ANN, RF, GBR and KRR under five-fold cross-validation. ANN exhibited the best overall predictive performance, achieving R^2 values of 0.99735, 0.99767, 0.99806 and 0.99573 for tensile strength, flexural strength, impact strength and Shore-D hardness, respectively. SHAP analysis was subsequently employed to interpret the selected ANN model. Jamun seed powder and *Prosopis juliflora* wood powder exhibited equal normalized predictive contributions of 50% each, reflecting their complementary compositional variation rather than independent causal effects. The combined experimental, ML and SHAP framework provides a systematic approach for evaluating composition-dependent performance and identifying promising hybrid epoxy biocomposites for lightweight engineering applications.

Keywords: Composite materials, Thermal Stability, Hardness, Machine Learning, SHAP analysis, ANN model

1. Introduction

Growing environmental concerns associated with petroleum-derived polymers and synthetic reinforcements have accelerated the development of sustainable biocomposites based on renewable lignocellulosic resources. Natural fibers and agro-waste-derived particulates are increasingly explored as reinforcements and fillers because of their low density, biodegradability, renewability, and favorable specific mechanical properties. Hybridization of different natural reinforcements can further improve composite performance by combining the structural contribution of fibers with the functional benefits of particulate fillers.

Natural-fiber hybrid composites reinforced with jute, snake grass, and kenaf fibers have demonstrated improved mechanical and wear performance. The incorporation of 5 wt.% *Annona reticulata* seed powder further reduced the wear rate of the hybrid composite (R. P. Kumar et al., 2022). *Annona reticulata*-derived biochar modified with chitosan achieved up to 94.37% azo-dye removal, while SEM, XRD, and FTIR analyses confirmed favorable structural

and surface characteristics for adsorption (Rajakumar et al., 2023). Annonaceae fruits have also been reported as nutrient-rich sources containing dietary fiber, minerals, and carotenoids (Brannan et al., 2025). Significant levels of phenolics, flavonoids, annonacin, and other bioactive metabolites have also been identified in *Annona reticulata* fruits and leaves (Shanmugam et al., 2024).

Prosopis juliflora is another abundantly available lignocellulosic resource with considerable potential for polymer composite development. Fine *Prosopis juliflora* fiber particles incorporated into PLA composites exhibited better tensile, flexural, and impact behavior than coarse particles, with 20 wt.% reinforcement producing optimum overall performance (Raj et al., 2020). Untreated and chemically treated *Prosopis juliflora* bark fibers were incorporated into epoxy composites at different fiber loadings, where chemical treatment improved fiber–matrix adhesion and mechanical properties, with 20 wt.% fiber providing optimum performance (Jena et al., 2022). Alkali treatment was also found to improve the interfacial bonding, crystallinity, thermal stability, and dynamic mechanical behavior of *Prosopis juliflora* fiber-reinforced composites (Reddy et al., 2022).

Hybridization of *Prosopis juliflora* with other natural reinforcements has further demonstrated significant property enhancement. Hybrid epoxy composites containing *Prosopis juliflora* bark, banana fiber, and coconut fiber exhibited improved tensile, flexural, compressive, impact, and hardness properties after alkali treatment due to enhanced fiber–matrix adhesion (S. S. Kumar & Raja, 2021). Alkali-treated *Grewia serrulata* and *Prosopis juliflora* fiber hybrid composites achieved approximately 48 MPa tensile strength at 30 wt.% reinforcement, together with improved wear resistance and reduced density (Nagarajan & Khan, 2026). Similarly, *Prosopis juliflora/Borassus flabellifer* fiber-reinforced epoxy composites containing tamarind-seed biofiller exhibited enhanced mechanical and tribological properties, with 2.5 wt.% filler providing favorable performance (Sandeep et al., 2026).

The incorporation of secondary fillers has also been investigated to improve the multifunctional behavior of *Prosopis juliflora*-based composites. Epoxy composites reinforced with 20 wt.% alkali-treated *Prosopis juliflora* fibers and $Mg(OH)_2/TiO_2$ nanofillers exhibited improved tensile, flexural, impact, thermal, fire-retardant, and moisture-resistant properties (Shalom et al., 2026). *Prosopis juliflora* ash used as a partial cement replacement at an optimum level of 20% improved compressive, tensile, flexural, elastic modulus, and impact properties while reducing environmental impacts (Govindaraj et al., 2025). Optimized pyrolysis of *Prosopis juliflora* biomass also produced a maximum biochar yield of 96.31%, demonstrating its potential for sustainable value-added applications (Ashwin et al., 2025).

Bio-based matrices derived from *Prosopis juliflora* have also received research attention. Jute-reinforced composites prepared using Mesquite gum derived from *Prosopis juliflora* and Plaster of Paris exhibited optimum tensile and flexural performance for the G60P40 composition, while G80P20 showed superior impact resistance (Dhamodharan & Gopalarama Subramaniyan, 2026). *Prosopis juliflora* leaf extract has additionally been utilized as a green reducing agent for preparing ZnO/SnO_2-rGO nanocomposites, which exhibited a specific capacitance of 128.43 F/g and 95.97% capacitance retention after 10,000 cycles (Govindasamy et al., 2025).

Syzygium cumini residues represent another promising class of sustainable biofillers. *Syzygium cumini* seed powder contained 43.28% cellulose, exhibited 42.63% crystallinity, and remained thermally stable up to 316.5 °C, supporting its suitability as a particulate

reinforcement for polymer composites (Thiagamani et al., 2024). Jamun-derived materials have also been incorporated into biodegradable packaging films, where the optimized formulation extended fruit storage up to 9 days (Tamane et al., 2026).

The novelty of this study lies in integrating a ternary natural-reinforcement system comprising *Annona reticulata* bark fibre, *Prosopis juliflora* wood powder and Jamun seed powder within an epoxy matrix with interpretable machine-learning analysis. Six APJ formulations with systematically varied wood-to-seed powder proportions were comprehensively assessed through mechanical, moisture, thermal, dynamic mechanical, structural and morphological characterization. Beyond experimental evaluation, ANN, RF, GBR and KRR were comparatively employed to predict tensile strength, flexural strength, impact strength and Shore-D hardness, with ANN identified as the best-performing model. A further distinctive aspect is the application of SHAP to the selected ANN model to interpret composition-dependent predictions. Rather than treating model accuracy alone as sufficient, the study quantifies the predictive contributions of the varying Jamun seed and *Prosopis juliflora* powder contents while explicitly accounting for their coupled compositional variation. Thus, the work combines hybrid bio-reinforcement development, multi-property characterization, ML prediction and explainable AI within a unified framework for composition-oriented epoxy biocomposite assessment.

2. Materials and methodology

2.1. Materials and preparation

Annona reticulata bark fibres, *Prosopis juliflora* wood and Jamun seeds were selected as the reinforcing constituents. LY556 epoxy and HY951 hardener formed the polymer matrix and were blended at a mass ratio of 10:1.

The wood was reduced to approximately 25–35 mm pieces, pulverized and sieved to obtain particles below 150 μm. Jamun seeds were cleaned, dehulled and processed into powder using the same size-selection procedure. Separated bark fibres were trimmed to a uniform length of 5 mm. Before chemical treatment, the reinforcing materials were sun-dried for 48 h. Figure 1 outlines the constituent preparation and composite production stages.

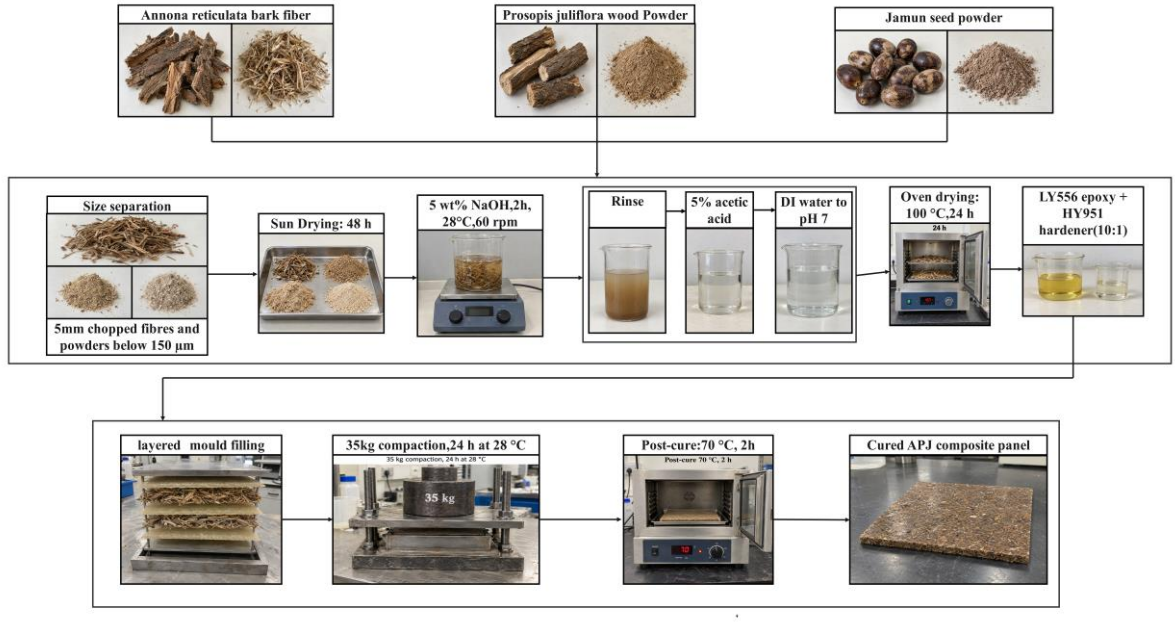

Fig. 1. Constituent materials and fabrication stages of hybrid epoxy composites.

2.2. Alkaline surface treatment

The three reinforcement materials were immersed in an aqueous solution containing 5 wt.% NaOH for 2hours at 28 °C, stirring maintained at 60 rpm. Following treatment, the materials underwent three tap-water rinses, neutralization with 5% acetic acid then subsequent washing with deionized water until the rinse reached pH 7.0 ± 0.1. Oven drying was then performed at 100 °C for 24 h.

This treatment was intended to remove surface contaminants and loosely bound non-cellulosic constituents while increasing surface roughness. These modifications were expected to support resin wetting and mechanical interlocking. Specific chemical-bonding mechanisms require confirmation through characterization.

2.3. Composite fabrication

Six formulations, APJ1–APJ6, were prepared using an open mold measuring 300 × 300 × 3 mm (Parvathamma et al., 2027). Polyvinyl alcohol and paraffin wax were applied to facilitate demolding. The bark-fibre proportion remained constant, whereas the wood-powder proportion decreased as the seed-powder proportion increased.

Table 1. Reinforcement proportions and mechanical-property values for APJ composites.

Sample	Annona proportion	Prosopis proportion	Jamun proportion	Tensile strength (MPa)	Flexural strength (MPa)	Impact strength (J/m)	Hardness (Shore D)
APJ1	42	38	6	188.4	231.6	15.2	64.3
APJ2	42	32	12	207.3	256.8	17.6	68.1

APJ3	42	26	18	228.6	284.7	20.1	72.6
APJ4	42	20	24	249.8	313.5	22.5	77.4
APJ5	42	14	30	267.4	341.2	24.7	81.8
APJ6	42	8	36	254.1	327.6	26.4	85.2

LY556 resin and HY951 hardener were mixed at 10:1 by mass and degassed before application (Bharat et al., 2026). A thin matrix layer was spread across the mould, followed by Jamun seed powder and another resin coating. Chopped bark fibres were distributed preferentially along one direction, followed by wood powder and an intermediate matrix layer. A second fibre layer was arranged in the perpendicular direction, after which the remaining powders and a final resin coating were introduced. A 35 kg compaction mass was applied during the initial 24 h curing period at 28 °C. The provisional post-curing schedule was 70 °C for 2 h. The resulting panels had a nominal thickness of 3 mm.

Maintaining the same bark-fibre proportion enabled comparison of the changing wood-to-seed powder balance. Consistent matrix content, fabrication conditions and specimen dimensions are necessary to interpret these comparisons; the matrix fraction must therefore be explicitly recorded.

The resulting architecture comprises epoxy layers containing short bark fibres and interspersed particulate fillers. It is described as a layered fibre–particulate hybrid composite. Fibre orientation, powder distribution, impregnation quality and interlayer adhesion provide the structural basis for interpreting its measured properties.

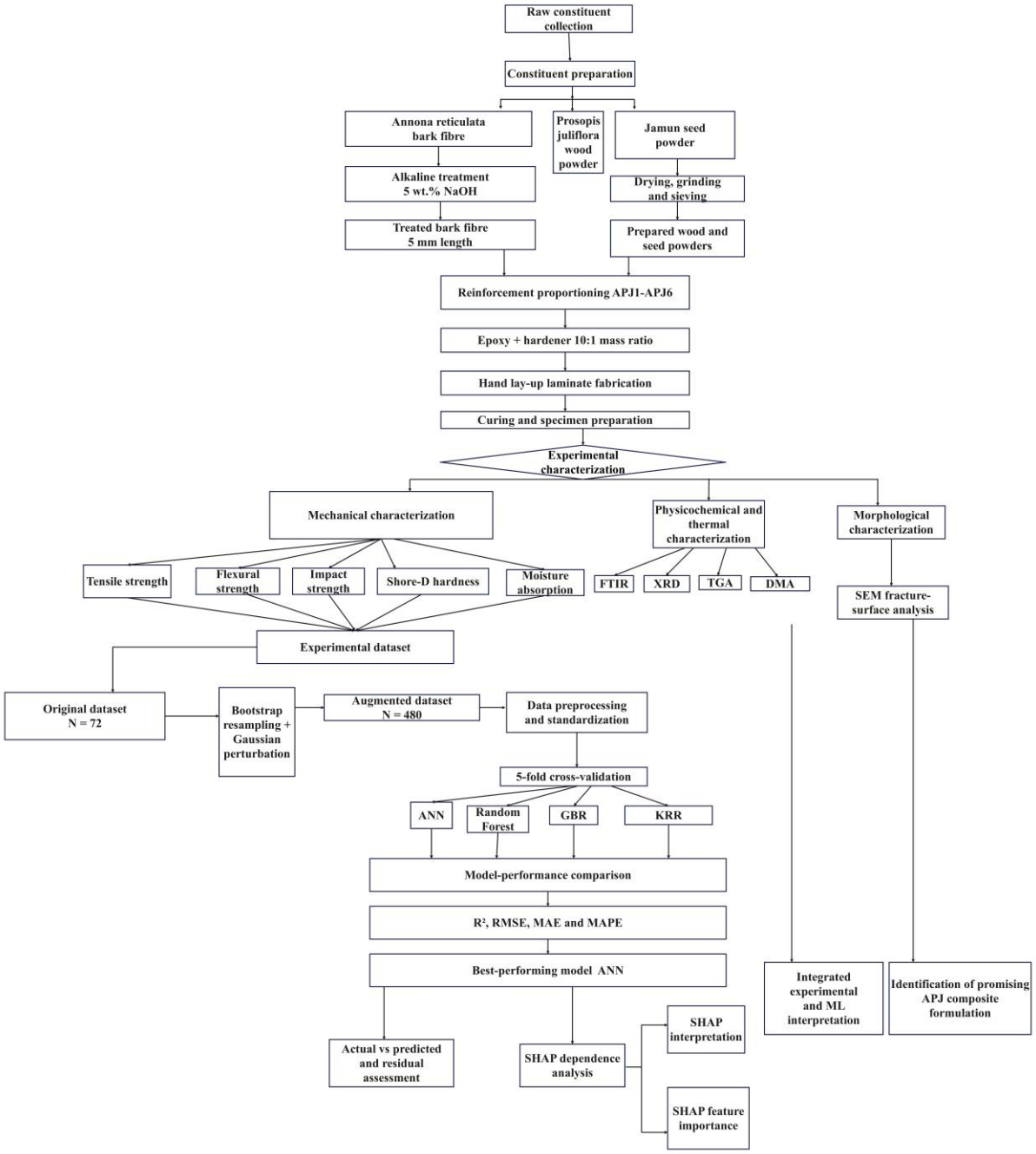

Fig. 2. Research sequence covering constituent preparation, alkaline treatment, laminate fabrication, mechanical and physicochemical characterization, dataset preparation, regression-model evaluation and SHAP interpretation.

2.4. Characterization

2.4.1. Mechanical testing

2.4.1.1. Tensile test

The Zwick Roell Z020 UTM with 20 kN load cell is proposed for tensile measurements following ASTM D638 (Kamble et al., 2026). Type I specimens, approximately 165 × 19 × 3 mm overall, will be loaded at 2 mm/min. Twelve independently tested specimens per

formulation provide the mean and 95% confidence interval. Tensile modulus was determined from the initial linear stress–strain response using extensometer measurements.

2.4.1.2. Three-point flexural testing

Zwick Roell Z020 with a three-point bending fixture following ASTM D790 was employed to find the flexural behaviour (Salins et al., 2026). Specimens measuring 125 × 13 × 3 mm will initially use a 48 mm support span, corresponding to a 16:1 span-to-thickness ratio. Crosshead speed will be calculated from the prescribed strain rate and actual dimensions. Twelve specimens will be evaluated per formulation with modulus calculated from the initial load–deflection slope.

2.4.1.3 Izod impact test

A HIT 5.5P pendulum tester fitted with an appropriate Izod hammer is proposed for ASTM D256 measurements (Jayarajan et al., 2026). Twelve notched specimens per formulation will be tested at 23 °C. Nominal dimensions will be 63.5 × 12.7 × 3 mm, incorporating a 45° notch and 0.25 mm root radius. Absorbed energy will be normalized according to the standard and reported in J/m.

2.4.1.4 Shore-D hardness

Hardness will be measured by Zwick Roell 3131 Shore D durometer following ASTM D2240 (Muin et al., 2025). Dedicated specimens of sufficient thickness will be prepared, targeting at least 6 mm. Five readings at separate locations will be collected with the required edge clearance and spacing. A consistent 15 s reading time will be documented.

2.5 Moisture absorption

Following ASTM D570, specimens will be dried to constant mass, cooled in a desiccator and weighed before immersion in deionized water at 23 °C. Measurements will continue daily for Fourteen days. Surface water will be removed consistently before weighing. Moisture uptake will be calculated as: MA (%) = [(Mt - M0)/M0] ×100.

2.6 SEM analysis

A Gemini, Zeiss scanning electron microscope is proposed for examining sputter-coated tensile fracture surfaces. Imaging at 5 kV and ×500 magnifications assess interfacial separation, fibre pull-out, particle distribution and voids.

2.7 Thermogravimetric analysis and degradation kinetics

A NETZSCH TG 209 F3 Tarsus will analyse approximately 10 mg of material from 30–700 °C at 10 °C/min at nitrogen flowing at 50 mL/min. Apparent degradation activation energy will be estimated using Broido relationship.

2.8. XRD, FTIR, and DMA

A Rigaku MiniFlex diffractometer will record XRD patterns using Cu Kα radiation over 5–80° with 0.02° increments. Crystallinity and coherent-domain estimates will account for overlapping constituent peaks. ATR-FTIR spectra will be collected using a Thermo Scientific Nicolet iS20 over 400–4000 cm^{-1} at 4 cm^{-1} resolution with 64 scans.

A NETZSCH DMA 242 E Artemis evaluate the specimens in a single-cantilever mode at 1 Hz, from −30 to 150 °C at 3 °C/min. Oscillation amplitude will remain within the linear viscoelastic range. Apparent effective crosslink density will be estimated from $\nu = E'/(3RT)$, using a stable rubbery plateau approximately 40-50 °C above (T_g). Reinforcement contributions to modulus will be acknowledged when interpreting this estimate.

2.9 Machine learning analysis

Machine-learning (ML) modelling was employed to predict the mechanical responses of the *Annona reticulata* bark fibre–*Prosopis juliflora* wood powder–Jamun seed powder reinforced epoxy composites. The overall procedure comprised dataset construction and augmentation, data preprocessing, five-fold cross-validation, development of ANN, RF, GBR and KRR models, performance evaluation and SHAP-based interpretation of the selected model.

2.9.1 Dataset preparation and augmentation

The ML dataset was constructed using the composition, processing conditions and measured mechanical responses of the APJ composite formulations. Eight parameters were initially defined as model inputs. The *Annona reticulata* bark fibre content was maintained at 42 wt.%, whereas *Prosopis juliflora* wood powder was varied from 38 to 8 wt.% and Jamun seed powder from 6 to 36 wt.%. The remaining parameters were fixed at 5 wt.% NaOH concentration, 5 mm fibre length, 10:1 epoxy-to-hardener ratio, 35 kg compaction load and 70 °C post-curing temperature. Tensile strength, flexural strength, impact strength and Shore-D hardness were considered as the four target responses.

The original dataset contained 72 observations, representing six APJ formulations with 12 observations for each formulation. To increase the number of observations available for model development, bootstrap resampling combined with small Gaussian perturbations was used to expand the dataset to 480 observations. During augmentation, the complementary relationship between Jamun seed powder and *Prosopis juliflora* wood powder was preserved, and constant compositional and processing parameters were kept unchanged. Small perturbations were also applied around the corresponding mechanical-response values to introduce local variability without substantially modifying the original response distributions.

The statistical similarity between the original and augmented datasets was examined using their mean and standard-deviation values. As shown in Table 2, only small differences occurred between the two datasets for all four mechanical responses, indicating that the augmentation retained the principal statistical characteristics of the original observations. The 480 observations were therefore used as synthetic model-development samples and were not considered additional independent experiments.

Table 2. Comparison of original and augmented datasets for ML development.

Metric	Original (N = 72)	Augmented (N = 480)
Mean TS (MPa)	232.60	231.91
Std. dev. TS (MPa)	27.85	28.44
Mean FS (MPa)	292.57	291.83
Std. dev. FS (MPa)	39.23	39.73
Mean IS (J/m)	21.08	20.96

Metric	Original (N = 72)	Augmented (N = 480)
Std. dev. IS (J/m)	3.93	3.92
Mean hardness (Shore-D)	74.90	74.70
Std. dev. hardness (Shore-D)	7.41	7.38

2.9.1.1. Data preprocessing and cross-validation

Before model development, the input matrix was examined for zero-variance predictors. *Annona reticulata* bark fibre content, NaOH concentration, fibre length, epoxy-to-hardener ratio, compaction load and post-curing temperature remained constant in the investigated dataset. Hence, *Prosopis juliflora* wood powder and Jamun seed powder constituted the effective varying composition parameters available for learning their relationship with the mechanical responses.

For algorithms requiring scaling, standardization was carried out using the mean and standard deviation calculated from the respective training fold:

$$z_i = \frac{x_i - \mu_x}{\sigma_x} \quad (1)$$

where x_i is the original value, μ_x and σ_x are the training-fold mean and standard deviation, respectively and z_i is the standardized value.

A five-fold cross-validation procedure was employed for all four ML models. The 480 observations were randomly partitioned into five folds. Four folds were used for training and the remaining fold for validation during each iteration. The process was repeated five times so that every observation served once as validation data. The validation predictions from all five folds were combined for calculation of the final performance metrics.

2.9.1.2 Machine-learning model development

Four regression models were evaluated: artificial neural network (ANN), random forest (RF), gradient boosting regression (GBR) and kernel ridge regression (KRR). A common five-fold cross-validation framework was maintained to permit direct comparison of their predictive performance.

The ANN was developed as a feed-forward multilayer network with an 8-12-8-4 architecture, consisting of eight conceptual input variables, two hidden layers containing 12 and 8 neurons, respectively, and four output neurons corresponding to the four mechanical properties. Hyperbolic tangent sigmoid activation functions were employed in the hidden layers, while a linear function was used for the output layer. Bayesian regularization was adopted for network training with a maximum of 1000 epochs and a performance goal of 1×10^{-7}.

RF was developed using an ensemble of 300 regression trees with a minimum leaf size of 3. GBR was implemented using the LSBoost algorithm with 250 learning cycles, a learning rate of 0.05, a minimum leaf size of 5 and a maximum of 10 splits. KRR employed a Gaussian radial basis function kernel with a regularization parameter of $\lambda = 0.10$ and a kernel parameter of $\gamma = 1.00$.

Table 3. Machine-learning models and principal model settings.

Model	Principal settings
ANN	8–12–8–4 architecture; Bayesian regularization; maximum 1000 epochs
RF	300 regression trees; minimum leaf size = 3
GBR	LSBoost; 250 learning cycles; learning rate = 0.05; minimum leaf size = 5; maximum splits = 10
KRR	Gaussian RBF kernel; λ=0.10\lambda=0.10; γ=1.00\gamma=1.00

2.9.1.3 Model performance evaluation

The predictive accuracy of ANN, RF, GBR and KRR was evaluated using the coefficient of determination (R^2), root mean square error (RMSE), mean absolute error (MAE) and mean absolute percentage error (MAPE). These parameters were calculated from the five-fold validation predictions as follows:

$$R^2 = 1 - \frac{\sum_{i=1}^{n}(y_i - \hat{y}_i)^2}{\sum_{i=1}^{n}(y_i - \bar{y})^2} \quad (2)$$

$$RMSE = \sqrt{\frac{1}{n}\sum_{i=1}^{n}(y_i - \hat{y}_i)^2} \quad (3)$$

$$MAE = \frac{1}{n}\sum_{i=1}^{n}|y_i - \hat{y}_i| \quad (4)$$

$$MAPE = \frac{100}{n}\sum_{i=1}^{n}\left|\frac{y_i - \hat{y}_i}{y_i}\right| \quad (5)$$

where y_i represents the actual value, $\hat{y}_i$ is the predicted value, $\bar{y}$ is the mean actual response and n is the total number of observations. The model showing the highest R^2 together with comparatively lower RMSE, MAE and MAPE was selected for further prediction analysis and SHAP interpretation.

2.9.2. SHAP analysis

SHapley Additive exPlanations (SHAP) analysis was applied to the selected ANN model to interpret the contribution of the varying composition parameters to the predicted mechanical responses. Since *Prosopis juliflora* wood powder and Jamun seed powder were the only predictors that varied across the investigated compositions, the SHAP dependence and feature-importance analyses were focused on these two variables. The remaining six parameters were constant and therefore provided no variation from which their individual predictive contributions could be estimated.

The ANN prediction was represented by the additive SHAP relationship:

$$f(x) = E[f(X)] + \sum_{j=1}^{M}\phi_j \quad (6)$$

where $E[f(X)]$ is the baseline ANN prediction, ϕ_j represents the SHAP contribution of the jth predictor and M is the number of active predictors. The global importance of each active predictor was determined using its mean absolute SHAP value:

$$I_j = \frac{1}{n}\sum_{i=1}^{n} |\phi_{ij}| \quad (7)$$

For comparison among mechanical responses having different units, the SHAP importance was normalized independently for each response:

$$I_{j,\,\mathrm{norm}} = \frac{I_j}{\sum_{k=1}^{M} I_k} \times 100 \quad (8)$$

SHAP dependence plots were used to examine how variations in Jamun seed powder and *Prosopis juliflora* wood powder influenced the ANN predictions, while mean absolute SHAP values were used to quantify their relative predictive importance. Since the two powder contents were varied complementarily in the APJ formulations, the SHAP values were interpreted as model-based predictive contributions within the investigated composition range rather than independent causal effects.

3.Results and discussion

3.1. Tensile property

Supplied dataset shows increasing tensile strength from 188.4 MPa for APJ1 to 267.4 MPa for APJ5, followed by a reduction to 254.1 MPa for APJ6. Intermediate strengths of 207.3, 228.6 and 249.8 MPa correspond to APJ2, APJ3 and APJ4, respectively. APJ5 therefore provides the highest tensile strength among the six evaluated formulations.

The increase accompanies the progressive replacement of *Prosopis juliflora* wood powder with Jamun seed powder at a constant *Annona reticulata* bark-fibre proportion. A possible explanation is a more favourable distribution of the particulate constituents around the fibres, supporting stress transfer through the epoxy matrix. However, the strength values alone cannot establish additional chemical crosslinking or specific interfacial bonding mechanisms.

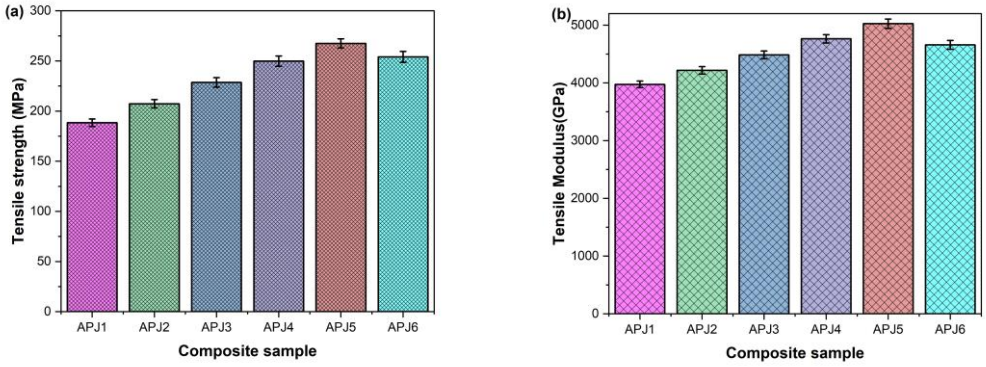

Figure 3. Tensile of APJ1–APJ6 hybrid epoxy composites: (a) TS, highlighting APJ5; (b) tensile modulus calculated from measured stress–strain data.

Relative to APJ1, APJ2, APJ3, APJ4 and APJ6, the tensile strength of APJ5 is higher by 41.93%, 28.99%, 17.00%, 7.05% and 5.23%, respectively. Moving from APJ5 to APJ6 produces a 4.97% strength reduction. This indicates that further increasing the seed-powder

proportion while decreasing the wood-powder proportion does not sustain the preceding improvement.

Particle clustering, incomplete impregnation or local interfacial separation could explain this reduction, but these possibilities require examination of the fracture surfaces. Because both powder proportions change together, their individual contributions cannot be separated using the present composition series.

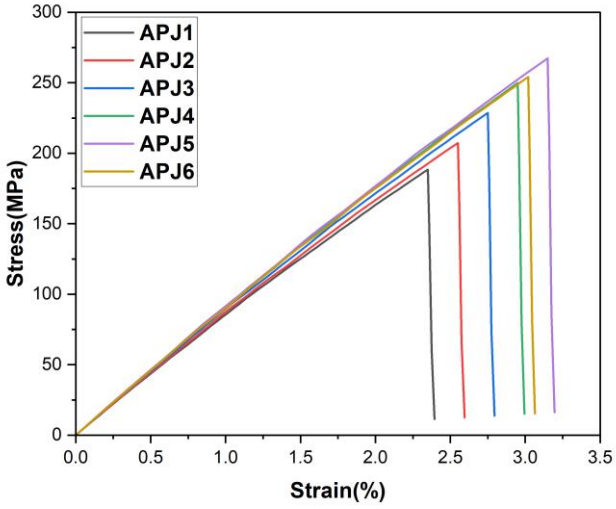

Fig. 4. Measured tensile stress–strain responses of APJ1–APJ6 hybrid epoxy composites.

Stress–strain measurements are necessary to determine stiffness, failure strain and deformation behaviour. Higher ultimate strength does not independently demonstrate greater ductility. Likewise, SEM evidence is required before attributing APJ5's performance to reduced voids or limited fibre pull-out. The available values identify APJ5 as the strongest formulation within this dataset; comparisons with published composites should account for differences in reinforcement content, specimen geometry and testing range.

3.2 Flexural property

FS increased from 231.6 MPa for APJ1 to 341.2 MPa for APJ5, representing a 47.32% improvement, before decreasing to 327.6 MPa for APJ6. APJ2, APJ3 and APJ4 exhibited intermediate values of 256.8, 284.7 and 313.5 MPa, respectively. This progression identifies APJ5 as the strongest formulation under bending within the supplied dataset.

The improvement toward APJ5 reflect more effective stress transfer and reinforcement distribution as the Jamun seed-powder proportion increases. However, enhanced crosslink density cannot be established from flexural strength alone. The 3.99% reduction from APJ5 to APJ6 could indicate local particle clustering or incomplete resin impregnation, subject to confirmation through morphological examination.

Flexural modulus must be calculated from the initial measured response; strength values alone cannot establish its variation. Prior research, that the jamun seed powder (JSP), bamboo cotton cloth (BCC), and E-glass fibre (EGF) reinforced epoxy composite achieved a flexural strength of 138.27 MPa, compared with 13.23 MPa for neat epoxy. This improvement resulted from effective hybrid reinforcement and enhanced load transfer (Ayyanar et al., 2026).

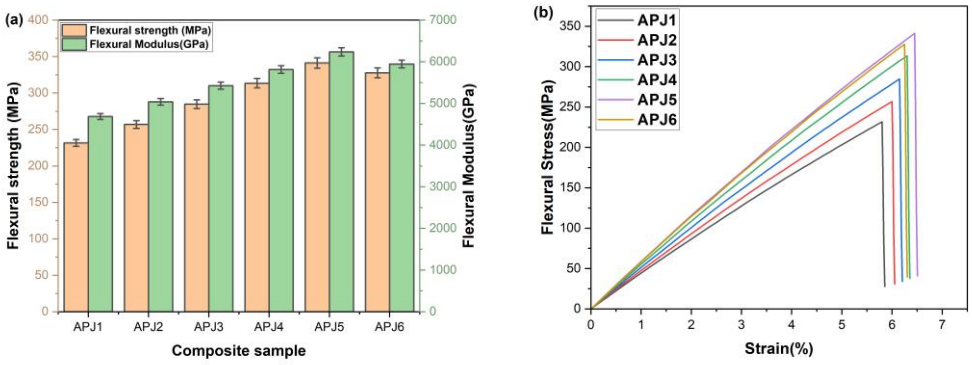

Fig. 5. Flexural response: (a) strength and modulus; (b) stress–strain curves.

3.3. IS and hardness

Impact strength raised consistently across APJ1–APJ6, with values of 15.2, 17.6, 20.1, 22.5, 24.7 and 26.4 J/m, respectively. APJ6 exceeded APJ1 by 73.68%. Unlike tensile and flexural strengths, which peaked at APJ5, impact resistance continued to increase in the final formulation.

This difference suggests that resistance to sudden loading and maximum strength respond differently to the changing powder balance. Interfacial separation, fibre pull-out and matrix deformation are possible energy-dissipation mechanisms, although their contributions require fracture-surface evidence.

Shore D hardness also increased progressively from 64.3 for APJ1 through 68.1, 72.6, 77.4 and 81.8 to 85.2 for APJ6. The trend indicates greater resistance to indentation as the Jamun seed-powder proportion rises. It does not independently demonstrate additional chemical crosslinking. Accordingly, APJ6 provides the highest impact resistance and hardness, whereas APJ5 retains the highest tensile and flexural strengths. In prior studies, demonstrated that, the optimized PJ bark–ramie fibre composite achieved an impact strength of 4.5 J and a hardness of 98 Shore D. The improvement was attributed to effective fibre–matrix bonding and enhanced cross-linking within the epoxy system (Arivendan et al., 2024).

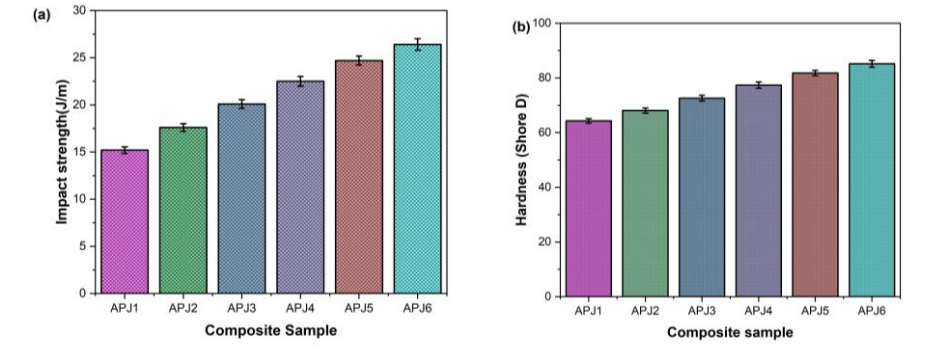

Fig. 6. APJ composites: (a) Izod IS; (b) Shore D.

3.4 Moisture absorption

Moisture behaviour of APJ1–APJ6 will be assessed from mass changes during ten days of water immersion. The comparison will distinguish the initial absorption rate from the eventual equilibrium uptake. Fickian behaviour will be considered only where the early response varies approximately approximately linearly with the square root of immersion time and subsequently approaches a stable plateau. A Fourteen-day measurement alone does not establish saturation. The *Annona reticulata* bark fibre, *Prosopis juliflora* wood powder and Jamun seed powder provide potential moisture-interaction sites within the epoxy composite. Their accessibility, together with impregnation quality and interfacial defects, may influence water uptake. However, the changing powder balance does not establish which formulation absorbs the least water without corresponding measurements.

APJ5 exhibits the highest tensile and flexural strengths in the supplied mechanical dataset, but this ranking cannot determine its moisture resistance. Absorption rate, equilibrium uptake and mechanical-property retention after conditioning should therefore be considered separately. Prior studies have confirmed that, the NaOH-treated Prosopis juliflora fibre composites exhibited lower moisture absorption than untreated composites due to reduced hydrophilicity and improved fibre–matrix bonding (Reddy et al., 2021).

Table 4. Moisture uptake of APJ1–APJ6 during water immersion and calculated diffusion coefficients.

Sample	First day	Third day	Five day	Seven day	Tenth day	Fourteen day	D (mm^2/s)
APJ1	1.18	2.04	3.16	3.91	4.48	4.62	2.72×10^{-6}
APJ2	1.1	1.91	3.01	3.73	4.28	4.41	2.78×10^{-6}
APJ3	1.02	1.78	2.84	3.53	4.06	4.18	2.82×10^{-6}
APJ4	0.94	1.64	2.66	3.32	3.83	3.96	2.83×10^{-6}
APJ5	0.86	1.49	2.45	3.08	3.58	3.72	2.78×10^{-6}
APJ6	0.98	1.71	2.76	3.45	3.96	4.09	2.85×10^{-6}

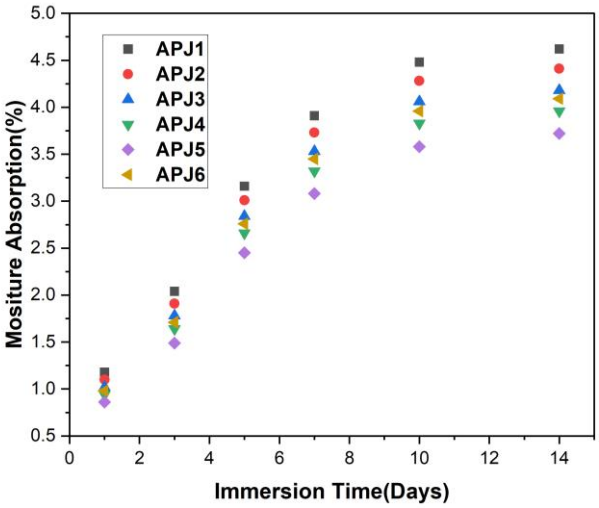

Fig. 7. Moisture absorption kinetics of APJ1–APJ6 hybrid biocomposites.

Diffusion coefficients will be derived using the initial absorption slope, specimen dimensions and an appropriate diffusion model. Comparisons must use consistent time and length units. Any relationship between crystallinity and moisture transport requires the corresponding APJ diffraction results; crystallinity alone cannot establish the absorption mechanism.

3.5 TGA and DTG analysis

APJ5 exhibits four thermal regions. Stage I extends from ambient temperature to 110 °C, with a mass loss of 4.0% associated with moisture release. Stage II includes the breakdown of less thermally stable constituents, with a characteristic temperature of 263 °C. During Stage III, spanning 320–440 °C, substantial polysaccharide decomposition occurs, producing the principal DTG maximum at 386 °C. Stage IV covers 440–550 °C and includes a broader degradation feature at 486 °C, provisionally associated with lignin-rich constituents and residual organic structures.

The jamun seed powder-containing APJ5 formulation achieves the highest decomposition onset temperature of 315 °C, residual char fraction of 17.3%, and apparent Broido activation energy of 63.4 kJ/mol. These results indicate delayed mass loss and increased residue formation without independently establishing a specific crosslinking mechanism. Table 5 summarizes the thermal parameters.

Table 5. Decomposition temperatures, residual char fractions and apparent activation energies determined using the Broido method.

Sample	T_{onset} (°C)	T_{10}% (°C)	T_{50}% (°C)	DTG T_{max} (°C)	Char yield	E_a (kJ/mol)	Stage II	Stage III
APJ1	287	252	389	374	11.8	52.7	200–305	305–425
APJ2	294	258	394	377	12.9	55.1	200–310	310–430
APJ3	301	266	399	380	14.1	57.8	200–315	315–435
APJ4	308	273	403	383	15.6	60.9	200–318	318–438
APJ5	315	279	407	386	17.3	63.4	200–320	320–440
APJ6	310	275	404	383	16.1	61.7	200–318	318–438

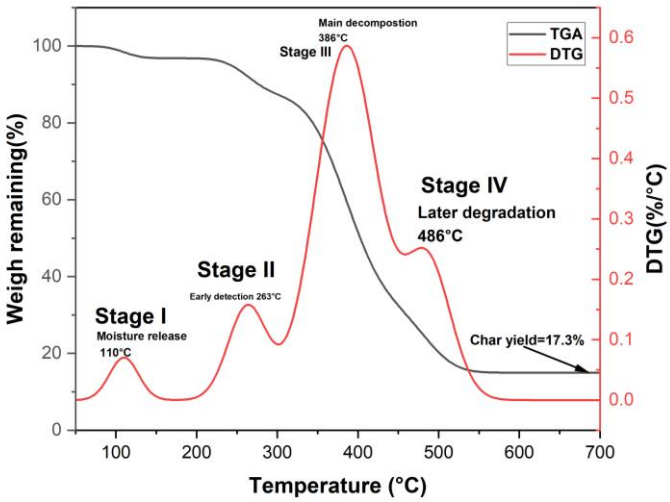

Figure 8. TGA and DTG profiles APJ5 under nitrogen at 10 °C/min, showing moisture release near 110 °C, early constituent degradation at 263 °C, the principal decomposition maximum at 386 °C, and a later degradation feature at 486 °C.

Among the investigated formulations, APJ5 demonstrates the greatest resistance to decomposition, with mass-loss onset at 315 °C and a char yield of 17.3% at 700 °C. Its thermal response is consistent with enhanced residue formation and delayed degradation. Prior investigations have shown that, the TGA revealed the thermal degradation behavior and stability of *Prosopis juliflora* bark, jute, and kenaf fibres. The analysis confirmed their suitability for polymer-composite processing within the observed thermal stability range (Muthalagu et al., 2021).

Activation energies were estimated using the Broido method from measurements collected at a single heating rate. Accordingly, these values provide model-dependent comparisons under the selected conditions and not interpreted as definitive kinetic parameters. Further analysis using multiple heating rates and isoconversional approaches, such as Kissinger–Akahira–Sunose or Flynn–Wall–Ozawa, would help evaluate conversion-dependent activation energies and clarify the decomposition behaviour.

3.6. FTIR spectroscopy

Figure 9 presents the functional-group characteristics of the APJ5 and APJ6 composites. The broad band at 3332 cm^{-1} is attributed to hydrogen-bonded O–H stretching in the *Annona reticulata* bark fibre and other lignocellulosic constituents. The absorption at 2923 cm^{-1} corresponds to aliphatic C–H stretching in cellulose and hemicellulose. The peak at 1734 cm^{-1} is assigned to carbonyl (C=O) stretching, while the band at 1605 cm^{-1} represents aromatic C=C vibrations associated with lignin. The peaks at 1425 cm^{-1} and 1238 cm^{-1} correspond to CH_2 deformation and C–O stretching, respectively. The strong band at 1032 cm^{-1} is attributed to C–O–C stretching in polysaccharide linkages, whereas the peak at 895 cm^{-1} indicates β-glycosidic linkages in cellulose.

The resemblance between the APJ5 and APJ6 spectra suggests comparable functional-group compositions. Consequently, their different mechanical responses can involve changes in reinforcement distribution, interfacial contact and internal porosity. Hydroxyl-band variations provide information about the local bonding environment but do not independently

demonstrate covalent attachment to epoxy. Table 7 lists the absorption bands and their assignments.

Table 6. FTIR absorption bands of APJ5 and APJ6 and corresponding APJ5 intensities.

Wavenumber (cm^{-1})	Functional group	Associated constituent	Vibrational mode
3332	O–H	Cellulose and absorbed water	Hydrogen-bonded hydroxyl stretching
2923	C–H	Cellulose and hemicellulose	Aliphatic C–H stretching
1734	C=O	Hemicellulose/matrix carbonyl groups	Carbonyl stretching
1605	C=C	Lignin aromatic structures	Aromatic skeletal vibration
1425	CH_2	Cellulose and hemicellulose	CH_2 deformation
1238	C–O	Lignin and polysaccharides	C–O stretching
1032	C–O–C	Cellulose and hemicellulose	Ether/glycosidic-bond stretching
895	C–H	Cellulose	β-Glycosidic-linkage vibration

Band annotations therefore identify O–H at 3332 cm^{-1}, C–H at 2923 cm^{-1}, C=O at 1734 cm^{-1}, aromatic C=C at 1605 cm^{-1}, CH_2 deformation at 1425 cm^{-1}, C–O at 1238 cm^{-1}, C–O–C at 1032 cm^{-1}, and β-glycosidic-linkage vibration at 895 cm^{-1}. Earlier research has indicated that, the FTIR confirmed the characteristic cellulose and hemicellulose functional groups in *Prosopis juliflora* bark powder. The identified bands support its lignocellulosic nature and suitability as a polymer-composite filler (Rathinavel et al., 2025).

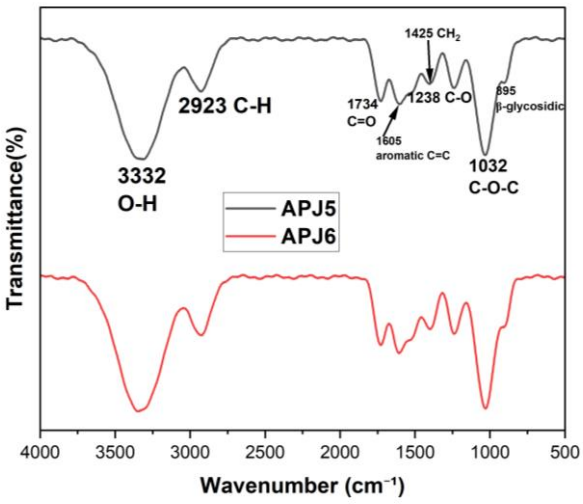

Fig. 9. ATR–FTIR spectra of APJ5 and APJ6 containing 40 wt% and 45 wt% jamun seed powder, respectively.

3.7.XRD analysis

APJ1–APJ4 diffraction patterns contain reflections around 2θ ≈ 16° and 22°. The APJ5 pattern shows distinct diffraction peaks at 15.8°, 22.3°, and 34.6°**,** indexed to the cellulose I planes (110), (200), and (004)**,** respectively. Table 8 presents the corresponding cellulose I and mixed cellulose I–II assignments.

The crystallinity index rises from 48.3% for APJ1 to 63.4% for APJ5. This increase is consistent with a greater relative contribution from ordered cellulose regions following the removal of amorphous constituents. Higher crystallinity accompanies improved stiffness, although interfacial adhesion and reinforcement arrangement also influence the mechanical response.

Table 7. Diffraction angles, interplanar distances, crystallite dimensions and crystallinity indices of APJ composites.

Sample	d-spacing 1 (Å)	d-spacing 2 (Å)	2θ peak 1 (°)	2θ peak 2 (°)	Crystallinity index (%)	Crystallite size (nm)
APJ1	5.75	4.07	15.4	21.8	48.3	3.33
APJ2	5.71	4.06	15.5	21.9	52.6	3.51
APJ3	5.68	4.04	15.6	22	56.1	3.68
APJ4	5.64	4.02	15.7	22.1	59.2	3.89
APJ5	5.61	3.98	15.8	22.3	63.4	4.12
APJ6	5.64	4	15.7	22.2	60.7	3.96

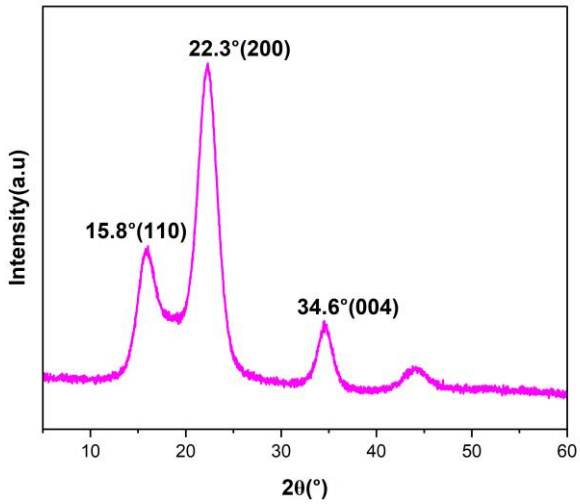

Fig. 10. XRD pattern and crystallinity index of APJ5 composite.

APJ5 exhibits Scherrer crystallite size of 4.12 nm. Its greater crystalline contribution corresponds with the enhanced mechanical response, supporting a relationship between

structural organization and reinforcement effectiveness. Previous studies revealed that, the XRD confirmed the crystalline characteristics of paraffin wax and aluminium within the *Prosopis juliflora* biochar-based PCM composites, with no significant new phases observed. This indicates good physicochemical compatibility among the composite constituents (Balasundaram & Sivaram, 2025).

3.8.DMA analysis

APJ5 displays the highest storage modulus, reaching 3.16 GPa at 30 °C, and therefore offers the greatest resistance to oscillatory deformation in the glassy region. The loss-modulus maximum places its glass-transition temperature at 80 °C. Across the formulations, Tg increases from 112 °C for APJ1 to 80 °C for APJ5 before decreasing to 104 °C for APJ6.

The initial increase is consistent with restricted polymer-segment movement arising from reinforcement–matrix interactions. At higher loading, changes in filler dispersion and matrix continuity can reduce this restriction. The resulting composition-dependent behaviour is reflected in the loss modulus, storage modulus and damping parameters presented in Table 8.

Table 8. Viscoelastic properties and apparent crosslink density of APJ composites.

Sample	E″ peak (MPa)	E′ at 30 °C	tan δ	Tg	Rubbery E′	Apparent crosslink density
APJ1	125.3	1.82	0.412	52	38.2	4.21
APJ2	148.7	2.14	0.389	58	44.6	4.87
APJ3	167.4	2.58	0.361	63	52.1	5.42
APJ4	189.6	2.97	0.334	70	61.8	6.18
APJ5	47.9	3.16	0.56	112	79.4	7.48
APJ6	41.7	2.82	0.66	104	60.3	5.68

APJ6 has a peak tan δ of 0.66, compared with 0.56 for APJ5. This reduction occurs despite its lower transition temperature, indicating that peak damping and Tg respond differently to composition. APJ5 combines the maximum storage modulus of 3.16 GPa with a Tg of 112 °C, demonstrating the strongest combination of glassy-state stiffness and resistance to temperature-induced softening within the investigated series

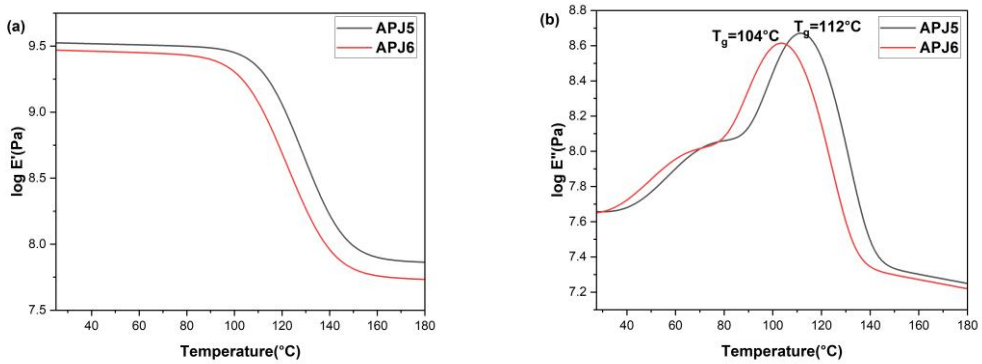

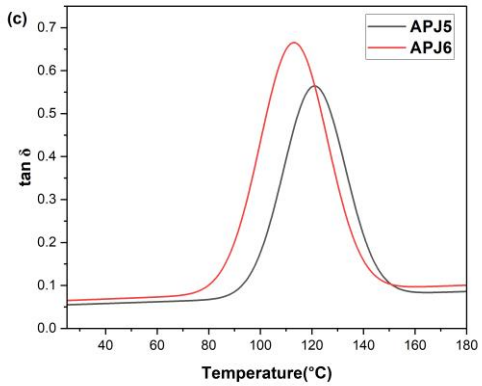

Fig. 11. Temperature-dependent DMA curves of APJ5 and APJ6: (a) logarithmic SM, log E′; (b) logarithmic LM, log E″; and (c) damping factor.

3.9.SEM analysis

Figure 12 presents the tensile-fracture morphologies of APJ1–APJ6. Figure 12 (a) shows fibre–matrix debonding, fibre breakage, matrix fracture and interfacial cavities, indicating weak stress transfer. Figure 12 (b) exhibits a rough fractured fibre surface with adhering matrix fragments, suggesting improved mechanical interlocking. Figure 12 (c) displays fibre damage, matrix cracking and river-pattern features associated with crack propagation. Figure 12 (d) contains particle agglomeration, deboned filler and matrix cracks, indicating locally non-uniform filler dispersion.

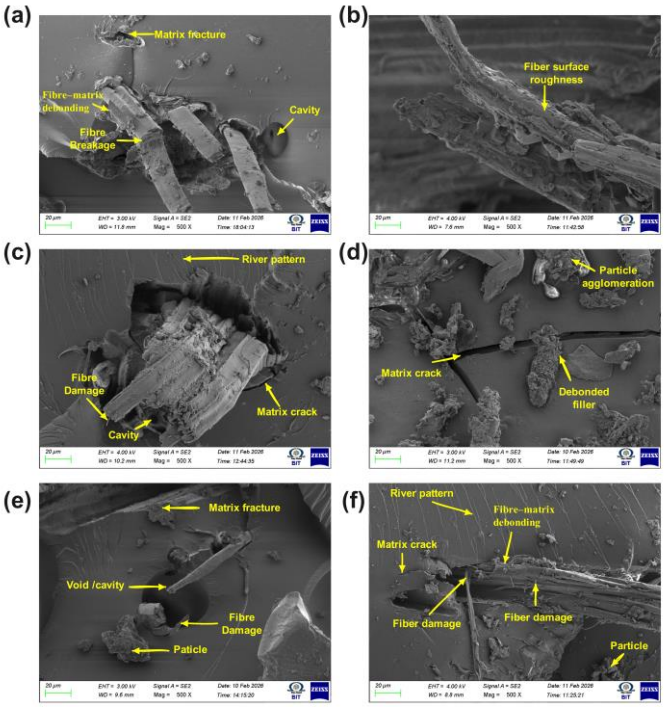

Figure 12. Tensile fracture morphology of (a) APJ1, (b) APJ2, (c) APJ3, (d) APJ4, (e) APJ5, (f) APJ6

Figure 12 (e) shows matrix fracture, fibre damage, dispersed particles and a visible void/cavity; nevertheless, the surrounding matrix remains relatively continuous. Figure 12 (f) exhibits extensive fibre damage, fibre–matrix debonding, matrix cracking, particles and pronounced river patterns, confirming unstable crack propagation and reduced tensile performance. In a prior study, SEM analysis revealed a distinct fibrillar and bundled surface morphology of *Annona reticulata* bark fibres, indicating the presence of well-defined cellulose fibrils. The relatively rough and irregular surface structure suggests favorable mechanical interlocking and interfacial adhesion when incorporated into polymer composites (Hossain et al., 2025).

3.10.ML Analysis

The predictive capability of four machine-learning models, namely artificial neural network (ANN), random forest (RF), gradient boosting regression (GBR) and kernel ridge regression (KRR) was compared for tensile strength, flexural strength, impact strength and Shore-D hardness of the *Annona reticulata* bark fibre–*Prosopis juliflora* wood powder–Jamun seed powder reinforced epoxy composites. All four models exhibited strong predictive performance under five-fold cross-validation with R^2 values above 0.994 for all four mechanical responses. However, differences in R^2 and prediction-error indices distinguished the relative performance of the models. Random Forest (RF) and Gradient Boosting Regression (GBR) for predicting radio propagation behavior in custard apple orchard environments. The models showed good predictive capability, although their performance decreased when extrapolating to unseen corridor geometries (Celades-Martínez et al., 2026).

For tensile strength, ANN achieved the highest R^2 of 0.99735, with RMSE, MAE and MAPE values of 1.4632 MPa, 1.1757 MPa and 0.52375%, respectively. GBR achieved the next highest R^2 of 0.99657, followed by RF at 0.99643 and KRR at 0.99639. A similar trend was observed for flexural strength, for which ANN produced the highest R^2 of 0.99767 and the lowest RMSE of 1.9160 MPa. RF and GBR both obtained R^2 values of 0.99723, whereas KRR produced an R^2 of 0.99661. As reported in previous studies, random Forest achieved a classification accuracy of 90.65%, with VARI, RVI, and red-edge bands identified as the most important predictive variables (Cherotich et al., 2026).

The highest predictive accuracy was obtained for impact strength, where ANN reached an R^2 of 0.99806, with RMSE and MAE values of only 0.17283 J/m and 0.13914 J/m, respectively. RF, GBR and KRR yielded R^2 values of 0.99778, 0.99775 and 0.99714, respectively. For Shore-D hardness, ANN again provided the highest R^2 of 0.99573, compared with 0.99527 for KRR, 0.99504 for GBR and 0.99487 for RF. The corresponding ANN RMSE and MAE were 0.48173 and 0.38343, respectively.

Table 9. Predictive performance of ANN, RF, GBR and KRR under five-fold cross-validation.

Mechanical response	Model	R^2	RMSE	MAE	MAPE (%)
Tensile strength	**ANN**	**0.99735**	**1.4632**	**1.1757**	**0.52375**
	RF	0.99643	1.6982	1.3492	0.60381
	GBR	0.99657	1.6630	1.3230	0.59300
	KRR	0.99639	1.7061	1.3479	0.59668
Flexural strength	**ANN**	**0.99767**	**1.9160**	**1.5094**	**0.52925**
	RF	0.99723	2.0907	1.6274	0.56980
	GBR	0.99723	2.0884	1.6249	0.57052

Mechanical response	Model	R^2	RMSE	MAE	MAPE (%)
	KRR	0.99661	2.3098	1.7841	0.62290
Impact strength	**ANN**	**0.99806**	**0.17283**	**0.13914**	**0.68133**
	RF	0.99778	0.18461	0.14961	0.73231
	GBR	0.99775	0.18594	0.15008	0.73445
	KRR	0.99714	0.20953	0.16448	0.80131
Shore-D hardness	**ANN**	**0.99573**	**0.48173**	**0.38343**	**0.51775**
	RF	0.99487	0.52802	0.41974	0.56565
	GBR	0.99504	0.51895	0.41244	0.55558
	KRR	0.99527	0.50663	0.40032	0.54088

Overall, ANN consistently produced the highest R^2 and lowest prediction errors across all four responses. The results therefore established ANN as the best-performing model among the four evaluated algorithms, and it was selected for subsequent prediction assessment and SHAP interpretation.

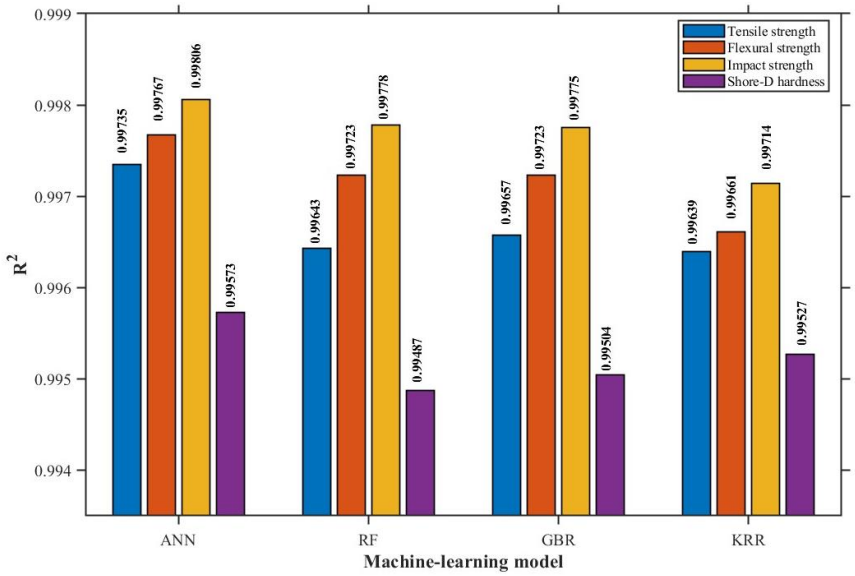

Fig. 13. Comparison of R^2 values of ANN, RF, GBR and KRR models for tensile strength, flexural strength, impact strength and Shore-D hardness prediction.

3.10.1. ANN Prediction Behaviour

The actual-versus-predicted responses of the ANN model showed close agreement for all four mechanical properties. The high R^2 values of 0.99735, 0.99767, 0.99806 and 0.99573 for tensile strength, flexural strength, impact strength and Shore-D hardness, respectively, indicate that ANN effectively represented the nonlinear relationship between the varying composite composition and the corresponding mechanical responses.

The relatively low RMSE and MAE values further support the agreement between actual and predicted responses. Among the investigated properties, impact strength exhibited the highest R^2 of 0.99806, while Shore-D hardness showed the comparatively lowest R^2 of 0.99573; nevertheless, the prediction accuracy remained high for both responses. The small

MAPE values, ranging from 0.51775% to 0.68133%, also demonstrate limited relative prediction error.

The ANN predictions reproduced the composition-dependent changes in the mechanical properties across the investigated formulations. Tensile and flexural strengths increased toward the higher-performing composition and reached maximum experimental values of 267.4 MPa and 341.2 MPa, respectively, for APJ5. A further change in composition in APJ6 reduced these values to 254.1 MPa and 327.6 MPa, respectively. In contrast, impact strength and Shore-D hardness continued to increase and reached their highest values of 26.4 J/m and 85.2 Shore-D, respectively, in APJ6. Thus, the different response trends were effectively represented by the ANN rather than assuming a common linear relationship for all mechanical properties.

The residual behaviour was consistent with the quantitative prediction metrics, with relatively small deviations between actual and ANN-predicted responses. The combined actual-versus-predicted and residual evaluation therefore confirms ANN as the most suitable of the investigated models for representing the mechanical-response trends within the studied composite formulation range.

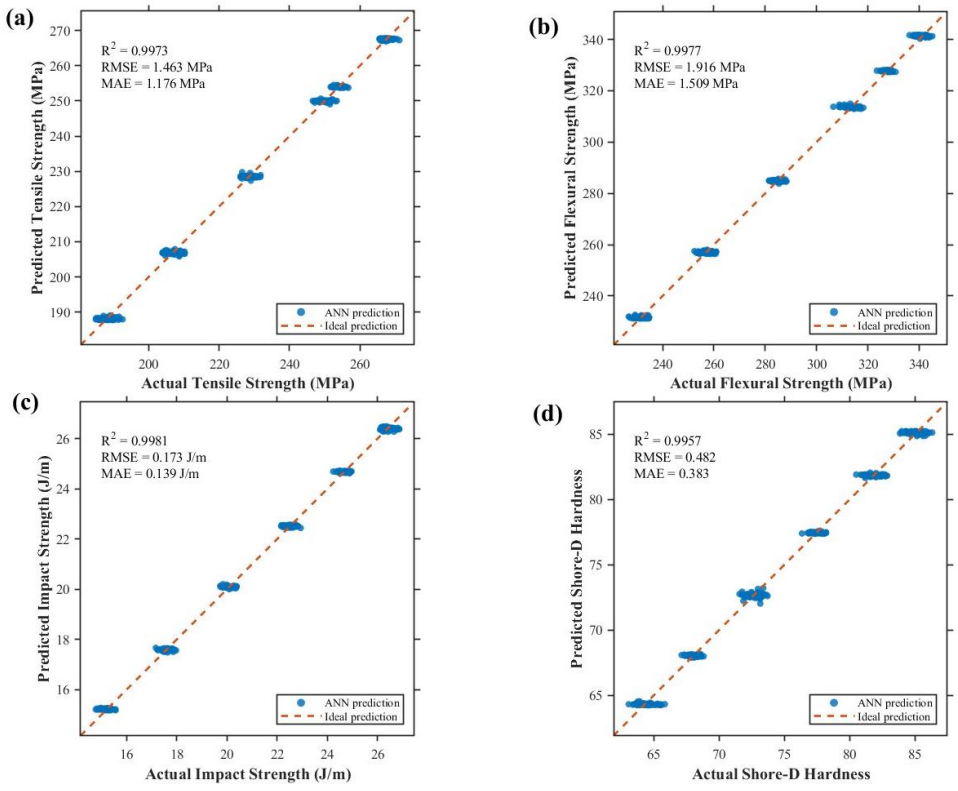

Fig. 14. Actual-versus-predicted responses and corresponding residual distributions of the ANN model for (a) tensile strength, (b) flexural strength, (c) impact strength and (d) Shore-D hardness.

3.11. SHAP Interpretation of the ANN Model

SHAP analysis was employed to interpret the predictions of the selected ANN model and to determine how the varying composition parameters contributed to the predicted mechanical responses. In the investigated dataset, Jamun seed powder and *Prosopis juliflora*

wood powder were the two varying composition parameters. Therefore, the SHAP dependence analysis focused on these two predictors.

For tensile-strength prediction, the SHAP dependence behaviour of Jamun seed powder changed progressively with its concentration. Lower Jamun seed powder contents were associated with negative SHAP contributions, whereas increasing Jamun content shifted the contribution toward positive SHAP values. This behaviour indicates that the progression toward higher Jamun seed powder content was associated with an increase in ANN-predicted tensile strength over a substantial part of the investigated range.

The *Prosopis juliflora* wood powder dependence plot exhibited the complementary trend. Higher *Prosopis* contents were associated with comparatively lower contributions to the ANN-predicted tensile response, while reducing its content shifted the SHAP contribution toward the positive region. This opposing behaviour is consistent with the formulation design, in which an increase in Jamun seed powder content was accompanied by a corresponding decrease in *Prosopis juliflora* wood powder content.

The SHAP dependence trends are also consistent with the nonlinear tensile response observed among the composite formulations. Tensile strength increased from 188.4 MPa in APJ1 to a maximum of 267.4 MPa in APJ5, followed by a decrease to 254.1 MPa in APJ6. Consequently, the ANN–SHAP analysis indicates that the composition-dependent tensile response was nonlinear rather than continuously increasing with the replacement of *Prosopis* powder by Jamun seed powder.

Because Jamun seed powder and *Prosopis juliflora* wood powder varied complementarily in the dataset, their individual SHAP effects should be interpreted as model-based predictive contributions within the investigated formulation space rather than as independent causal effects.

3.11.1. SHAP Feature Importance

The mean absolute SHAP values were used to quantify the contribution of the varying composition parameters to the ANN predictions. For tensile-strength prediction, Jamun seed powder and *Prosopis juliflora* wood powder each exhibited a mean absolute SHAP value of 12.4803 MPa. Their normalized feature contributions were therefore 50.0% each.

Table 10. SHAP feature importance of the varying composition parameters in the ANN model.

Predictor	Tensile mean SHAP (MPa)	Tensile contribution (%)	Flexural contribution (%)	Impact contribution (%)
Jamun seed powder	12.4803	50.0	50.0	50.0
Prosopis juliflora wood powder	12.4803	50.0	50.0	50.0

The normalized SHAP analysis similarly assigned 50% contribution to each varying predictor for flexural and impact-strength predictions. This equal attribution arises from the complementary variation of Jamun seed powder and *Prosopis juliflora* wood powder in the investigated compositions. Hence, the 50:50 SHAP distribution does not establish that the two

powders possess identical intrinsic effects on mechanical performance; rather, it reflects how the ANN distributes predictive contribution between the two coupled composition variables.

The other model inputs, including *Annona reticulata* bark fibre content, NaOH concentration, fibre length, epoxy-to-hardener ratio, compaction load and post-curing temperature, remained constant across the investigated dataset. Consequently, no variation was available for SHAP to estimate their individual predictive contributions, and their SHAP values were zero. The feature-importance interpretation was therefore restricted to the two composition variables that changed among the investigated formulations.

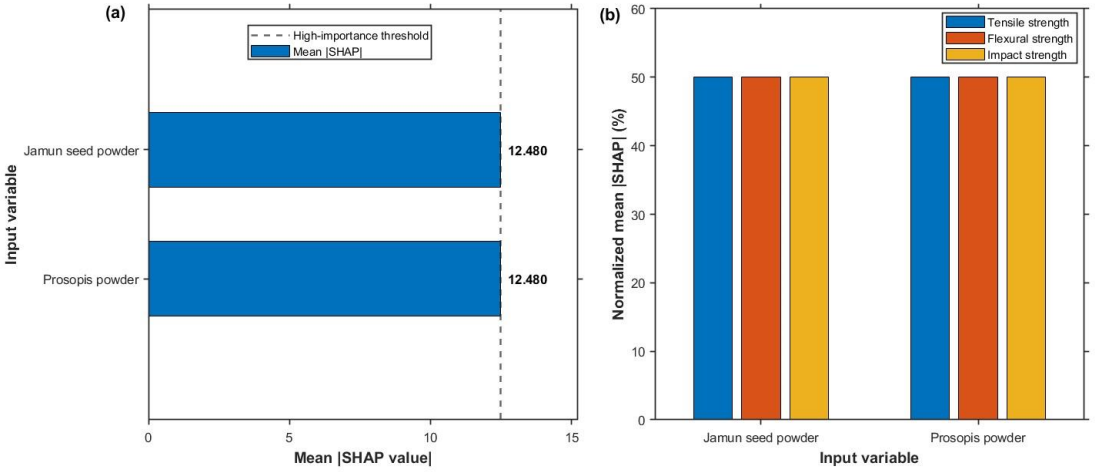

Figure 15. SHAP analysis of the ANN: (a) mean absolute SHAP values of Jamun seed powder and *Prosopis juliflora* wood powder for tensile-strength prediction and (b) normalized SHAP contributions of the two varying composition parameters for tensile, flexural and impact-strength predictions.

4. Conclusions

The present study developed and evaluated a ternary epoxy biocomposite reinforced with Annona reticulata bark fibre, Prosopis juliflora wood powder and Jamun seed powder through mechanical, thermal, dynamic mechanical, morphological and machine-learning analyses. The experimental results demonstrated a clear composition-dependent response among the APJ formulations. APJ5 exhibited the highest tensile and flexural strengths of 267.4 MPa and 341.2 MPa, respectively, identifying it as the optimum formulation for static mechanical performance. Its superior performance was supported by improved reinforcement–matrix interaction, fewer interfacial defects and favourable thermal and dynamic mechanical characteristics. In contrast, the reduction in tensile and flexural strengths observed for APJ6 was associated with localised filler agglomeration and interfacial debonding at the higher powder-loading condition.

Machine-learning analysis was performed using ANN, RF, GBR and KRR under a common five-fold cross-validation framework. Among these models, ANN exhibited the best overall predictive performance, with R^2 values of 0.99735, 0.99767, 0.99806 and 0.99573 for tensile strength, flexural strength, impact strength and Shore-D hardness, respectively. The corresponding low prediction errors confirmed close agreement between the actual and ANN-predicted responses. Consequently, ANN was selected for model interpretation using SHAP analysis.

SHAP interpretation showed that Jamun seed powder and *Prosopis juliflora* wood powder were the active varying composition parameters governing the ANN predictions within the investigated dataset. Their normalized SHAP contributions were 50% each, reflecting their complementary variation across the APJ formulations. Therefore, these SHAP contributions represent model-based predictive importance rather than independent causal effects. The other compositional and processing parameters were maintained constant and hence could not be independently ranked by SHAP.

Overall, the integration of experimental characterization, machine-learning prediction and SHAP interpretation provided an effective framework for evaluating and interpreting the performance of the developed hybrid epoxy biocomposites. The findings identify APJ5 as the most promising formulation for high tensile and flexural performance within the investigated composition range. However, the augmented dataset represents synthetic model-development observations rather than additional independent experiments. Further studies involving additional independently manufactured formulations and external validation datasets are therefore required to assess the broader generalisation and engineering applicability of the developed predictive framework.

References

Arivendan, A., Keerthiveettil Ramakrishnan, S., Chen, X., Zhang, Y.-F., Gao, W., Syamani, F. A., Thangiah, W. J. J., & Siva, I. (2024). Extraction and characterization of novel Prosopis Juliflora bark and Boehmeria nivea fibre for use as reinforcement in the hybrid composites with the effect of curing temperature, fibre length and weight percentages. *International Journal of Biological Macromolecules*, *279*. https://doi.org/10.1016/j.ijbiomac.2024.135093

Ashwin, R., MercyVasan, A., & Subramanian, K. (2025). Production and characterization of biochar from agro-forestry-based waste Prosopis juliflora: a sustainable amendment for soil conditioning. *Biomass Conversion and Biorefinery*, *15*(13), 20347–20364. https://doi.org/10.1007/s13399-025-06613-6

Ayyanar, C. B., Sivarathinamoorthy, H., Kenned, J. J., Helaili, S., Kumar, N., Mordovian, A. K., Kytinou, V., Sankar, M., Jeffrin, V., Pramod, P., Logesh, M., Padmanaban, P. S., Thomas, S., Pillai, P., Hilal, R., & Parveen, G. (2026). Sustainable hybrid epoxy sandwich composites reinforced with jamun seed powder, bamboo cotton, and E-glass fibres: experimental and FEM-based mechanical characterization. *Iranian Polymer Journal (English Edition)*. https://doi.org/10.1007/s13726-026-01728-7

Balasundaram, P., & Sivaram, N. M. (2025). Sustainable thermal energy management for electronic devices: A study on paraffin wax, biochar, and aluminium composite phase change materials. *Journal of Energy Storage*, *132*. https://doi.org/10.1016/j.est.2025.117686

Bharat, N., Subramanian, L. R. G., & Saravanakumar, K. (2026). Effect of Fiber Hybridization on Mechanical Behavior of Hybrid Composite Laminates. *Polymer Composites*, *47*(17), 16057–16068. https://doi.org/10.1002/pc.71341

Brannan, R., O'neal, D., & Jawad, M. (2025). Characterization of carotenoids and color in temperate Asimina triloba and comparison to other tropical Annonaceae fruits. *Exploration of Foods and Foodomics*, *3*. https://doi.org/10.37349/eff.2025.101098

Celades-Martínez, J., Diago-Mosquera, M. E., Peña, A., & García, J. (2026). Shadow fading prediction at 18 GHz through physics guided learning in vegetative corridors. *Scientific Reports*, *16*(1). https://doi.org/10.1038/s41598-026-36878-4

Cherotich, F., Galgallo, D., Dhulipala, R., Whitbread, A., & Paliwal, A. (2026). Tracking Rangeland Degradation from Prosopis juliflora Invasion in Kenya: A Multi-Source Approach Combining Remote Sensing, Machine Learning, and Citizen Science. *Ecologies*, *7*(1). https://doi.org/10.3390/ecologies7010020

Dhamodharan, S., & Gopalarama Subramaniyan, G. (2026). Influence of resin composition on mechanical properties of eco-friendly jute-mesquite gum and POP composites. *Journal of Reinforced Plastics and Composites*, *45*(7–8), 1781–1798. https://doi.org/10.1177/07316844251337335

Govindaraj, B. B., Sivamani, J., Palsamy, G., Raja, S., Zema, T. B., Balakrishnan, S., & Ramesh, A. (2025). Prosopis juliflora ash – Novel discussion as replacement to cement in the production of sustainable concrete. *Case Studies in Construction Materials*, *23*. https://doi.org/10.1016/j.cscm.2025.e05296

Govindasamy, S., Vaiyapuri, N., Suriyamoorthy, U., S. J, B. J., Natarajan, B., Varatharajan, B., Britto, P. G. J., & Anbazhagan, G. K. (2025). One-pot green bio-assisted synthesis of ZnO/SnO2-rGO hybrid nanocomposites using Prosopis juliflora leaf extract for high-performance supercapacitor electrode. *Journal of Organometallic Chemistry*, *1041*. https://doi.org/10.1016/j.jorganchem.2025.123842

Hossain, S., Saeed, M. A., Islam, T., Islam, S., Jalil, M. A., Rahman, M. M., & Das, S. C. (2025). Characterization of novel Annona reticulata fiber as a potential reinforcement for composite applications. *Scientific Reports*, *15*(1). https://doi.org/10.1038/s41598-025-15601-9

Jayarajan, N., Hong, T. W., & Ganesan, T. (2026). Thermal, mechanical, and sound absorption properties of sugarcane bagasse–rice husk hybrid polymer composites. *International Journal of Automotive and Mechanical Engineering*, *23*(2), 13601–13616. https://doi.org/10.15282/ijame.23.2.2026.10.1029

Jena, P. K., Samal, P., Nayak, S., Behera, J. R., Khuntia, S. K., Mohapatra, J., Mohanty, S. D., & Malla, C. (2022). Experimental Investigation on the Mechanical, Thermal, and Morphological Behaviour of Prosopis juliflora Bark Reinforced Epoxy Polymer Composite. *Journal of Natural Fibers*, *19*(14), 8593–8603. https://doi.org/10.1080/15440478.2021.1964144

Kamble, P. D., Satishkumar, P., Selvapandian, D., Saminathan, R., Singh, P., Natarajan, N., & Chelliah, A. (2026). Mechanical and low-velocity impact behavior of rGO-reinforced woven Agave americana fiber polyethylene composites. *Interactions*, *247*(1). https://doi.org/10.1007/s10751-026-02494-x

Kumar, R. P., Muthukrishnan, M., & Sahayaraj, A. F. (2022). Experimental investigation on jute/snake grass/kenaf fiber reinforced novel hybrid composites with annona reticulata seed filler addition. *Materials Research Express*, *9*(9). https://doi.org/10.1088/2053-1591/ac92ca

Kumar, S. S., & Raja, V. M. (2021). Processing and determination of mechanical properties of Prosopis juliflora bark, banana and coconut fiber reinforced hybrid bio composites for an engineering field. *Composites Science and Technology*, *208*. https://doi.org/10.1016/j.compscitech.2021.108695

Muin, N. F. A., Zakaria, N. H., Taha, M. M., Jumaidin, R., & Arbintarso, E. S. (2025). Characterization of Mechanical, Physical and Chemical Properties on Thermoplastics Cornstarch Composite Reinforced by Alkaline Treated Coconut Husk Fibre. *Jurnal Kejuruteraan*, *37*(8), 3809–3825. https://doi.org/10.17576/jkukm-2025-37(8)-13

Muthalagu, R., Srinivasan, V., Sathees Kumar, S., & Krishna, V. M. (2021). Extraction and Effects of Mechanical Characterization and Thermal Attributes of Jute, Prosopis Juliflora Bark and Kenaf Fibers Reinforced Bio Composites Used for Engineering Applications. *Fibers and Polymers*, *22*(7), 2018–2026. https://doi.org/10.1007/s12221-021-1092-9

Nagarajan, A., & Khan, A. (2026). Fabrication and mechanical characterization of alkali-treated Grewia serrulata and Prosopis juliflora fiber reinforced epoxy bio-composites. *Interactions*, *247*(1). https://doi.org/10.1007/s10751-026-02674-9

Parvathamma, P. K. S., Kumshikar, R. R., Adeppa, A., Muniswamy, T. K., & Gurbasappa, S. S. (2027). Experimental Study of Woven Glass, Bamboo, and Jute Fibre Reinforced in Epoxy Composites. *Mechanics of Advanced Composite Structures*, *14*(1), 41–56. https://doi.org/10.22075/MACS.2025.37201.1821

Raj, S. S., Kannan, T. K., & Rajasekar, R. (2020). Influence of prosopis juliflora wood flour in poly lactic acid - Developing a novel bio-wood plastic composite. *Polimeros*, *30*(1). https://doi.org/10.1590/0104-1428.00120

Rajakumar, S., Ramakrishnan, S., Monica Nandini, G. K., El-Marghany, A., Warad, I., & Kumar, M. S. (2023). Valorization of annona reticulata biochar by chitosan for the adsorption of azo dye from textile effluent. *Global Nest Journal*, *25*(6), 109–118. https://doi.org/10.30955/gnj.004882

Rathinavel, S., Saravanakumar, S. S., Prithviraj, M., Dhanamurugan, A., Karthikeyan, J., Banu, T., & Selvapreethi, G. (2025). Examining the Potential for Employing Biowaste Prosopis juliflora Bark as an Additive in Particulate-Reinforced Polymer Based Composite Materials. *Waste and Biomass Valorization*, *16*(3), 1073–1083. https://doi.org/10.1007/s12649-024-02726-7

Reddy, P. V, Mohana Krishnudu, D., Rajendra Prasad, P., & R, V. S. R. (2021). A Study on Alkali Treatment Influence on Prosopis Juliflora Fiber-Reinforced Epoxy Composites. *Journal of Natural Fibers*, *18*(8), 1094–1106. https://doi.org/10.1080/15440478.2019.1687063

Reddy, P. V, Reddy, R. V. S., Reddy, B. V, Krishnudu, D. M., Prasad, P. R., & Rao, P. S. (2022). Enhancement of the Dynamic Mechanical and Dielectric Properties of Prosopis juliflora Fiber-Reinforced Composites by Fiber Modification. *Journal of Natural Fibers*, *19*(13), 6780–6796. https://doi.org/10.1080/15440478.2021.1932676

Salins, S. S., Shetty, S., Doreswamy, D., Gowda, T., & Sachidananda, H. K. (2026). Flexural performance and microstructural correlation of natural silk fabric-reinforced epoxy composites. *Scientific Reports*, *16*(1). https://doi.org/10.1038/s41598-026-55528-3

Sandeep, V., Pant, R., Elanchezhian, J., Sankar, T., Kaliappan, S., & Prabhakaran, S. (2026). Hybrid composites enhancing mechanical and wear performance using Prosopis Juliflora and Borassus Flabellifer fibers with tamarind seed bio-filler. *Interactions*, *247*(1). https://doi.org/10.1007/s10751-026-02571-1

Shalom, N., Haridass, R., Kulurkar, P., & Mayakannan, S. (2026). Development of Eco-Friendly Prosopis Juliflora Fiber-Reinforced Epoxy Composites with Mg (OH)2 and TiO2 Nanofillers for Improved Mechanical and Fire-Retardant Properties. *International Research Journal of Multidisciplinary Technovation*, *8*(4), 288–306. https://doi.org/10.54392/irjmt26417

Shanmugam, H., Biswal, B. K., Sundaresan, S., Selvakumar, D., Kennedy, Z. J., & Priya, R. S. (2024). Comparative nutrient and chemometric analysis of leaf to fruits of Sourpsop (Annona muricata) and Bullock's heart (Annona reticulata): Implications for nutraceutical development. *Journal of Food Composition and Analysis*, *135*. https://doi.org/10.1016/j.jfca.2024.106686

Tamane, A., Chim, P., Shaikh, N., & Shaik, L. (2026). Biodegradable agar-based films with natural extracts for extending the shelf life of jamun (Syzygium cumini). *Journal of Food Measurement and Characterization*, *20*(3), 3205–3217. https://doi.org/10.1007/s11694-025-03810-9

Thiagamani, S. M. K., Yaswanth, C. V, Yashwanth, C., Tran, T. M. N., Krishnasamy, S., Azhaguchamy, M., Khan, A., Hashem, M., & Fouad, H. (2024). Characterization of Syzygium cumini (L.) Skeels (Jamun Seed) Particulate Fillers for Their Potential Use in Polymer Composites. *Molecules*, *29*(11). https://doi.org/10.3390/molecules29112618